

Theoretical study of the magnetic properties of the CoCu_2O_3 compound

Julien L ev eque ^{1,2}, Elisa Rebolini ³, Marie-Bernadette Lepetit ^{2,3,*} and Andr es Sa ul ^{1,†}

¹Centre Interdisciplinaire de Nanoscience de Marseille, CNRS UMR 7325, 13288 Marseille, France

²Institut N eel, CNRS UPR 2940, 38042 Grenoble, France

³Institut Laue Langevin, 38042 Grenoble, France



(Received 6 September 2022; accepted 14 November 2022; published 5 December 2022)

In this paper we present a theoretical study of the magnetic properties of the CoCu_2O_3 compound. The magnetic effective exchange interactions and zeroth-field splitting were computed using *ab initio* methods, then the magnetic order and transition temperature were determined using classical Monte Carlo simulations. We showed that, unlike other members of the ACu_2O_3 family, the presence of an additional magnetic atom, associated with a large folding of the puckered layers in the (\vec{a}, \vec{b}) directions, induces a magnetic pattern based on coupled three-leg ladders, quite different from the two-leg structural ladders. The propagation vector has been found to be $\vec{q} = (0, \frac{1}{2}, \frac{1}{2})$. It is associated with a doubly degenerated ground state suggesting a doubling of the unit cell. The large Co^{2+} -ion anisotropy was shown to be of crucial importance in the high transition temperature observed in this compound.

DOI: [10.1103/PhysRevB.106.224402](https://doi.org/10.1103/PhysRevB.106.224402)

I. INTRODUCTION

Following the discovery of high-temperature superconductivity in $\text{Ba}_x\text{La}_{5-x}\text{Cu}_5\text{O}_{5(3-y)}$ by Bednorz and M uller [1], cuprates have attracted a lot of attention over the past decades. Apart from superconductivity, a large number of compounds of the cuprate family have been studied for their low-dimensional quantum magnetism. Indeed, the $S = 1/2$ character of the Cu^{2+} ion, and the directionality of the associated $3d$ magnetic orbital, are responsible for a tendency to form one-dimensional (1D) or two-dimensional magnetic systems with quantum character. For example, the $A = \text{Sr}$ member of the ACu_2O_3 family, a two-leg ladder compound, has been extensively studied in the recent decades [2–8] for its one-dimensional properties.

Very few cuprates exhibit a three-dimensional (3D) magnetic ordering at a reasonable temperature (i.e., close to room temperature or higher). Among them, one can, however, cite the CuO oxide that exhibits an antiferromagnetic long-range ordering below 220 K [9,10]. Another example is the $A = \text{Mg}$, Ca , and Co members of the ACu_2O_3 family that exhibit a high-temperature 3D character, and that, in contrast to CuO , have been little studied. Interestingly, the MgCu_2O_3 compound presents a 3D spin ordering at 95 K [11], and the mixed $\text{Ca}_{1-x}\text{Co}_x\text{Cu}_2\text{O}_3$ compounds show ordering temperatures that range from 27 K for pure Ca ($x = 0$) [12] to 215 K for pure Co ($x = 1$) [13].

The room-temperature crystal structure of this family is orthorhombic ($Pm\bar{m}n$ or $Cmmm$). The copper atoms are located at the center of CuO_4 corner-sharing square plaquettes, arranged in two-leg ladders along the \vec{b} direction [see Fig. 1(a)].

In each unit cell there are two symmetry-related ladders along the \vec{a} direction (represented in blue and green). These two-leg copper ladders are zigzag coupled, and form planar (Sr compound) or puckered (Mg , Ca , and Co) layers in the (\vec{a}, \vec{b}) directions [see Fig. 1(b)]. These layers are connected along the \vec{c} direction, by AO_6 octahedra ($A = \text{Mg}$, Ca , Co), or AO_8 cubes ($A = \text{Sr}$), sharing corners with the CuO_4 plaquettes from adjacent copper-ladder layers [see Fig. 1(b)].

At this point one should note that the Sr compound also differs from the Mg , Ca , and Co ones by its magnetic properties. Indeed, whereas the latter ones present a 3D magnetic order below its N eel temperature, the Sr compound remains essentially 1D [3]. It, thus, seems that the puckering of the (\vec{a}, \vec{b}) layers plays a major role in the dimensionality of the magnetic ordering.

In this article we will study the magnetic properties of the CoCu_2O_3 compound, the member of the ACu_2O_3 family with the highest-3D-ordering temperature. After the evaluation of the effective exchange interactions using *ab initio* calculations, we will compute the associated magnetic order by classical Monte Carlo (MC) methods.

This paper is organized as follows. Section II details the computational methods. Section III is devoted to the calculations of the exchange interactions and single-ion anisotropy. In Sec. IV we discuss the magnetic order at zero and finite temperatures. Finally, we conclude in Sec. V.

II. COMPUTATIONAL DETAILS

A. *Ab initio* calculations

As the magnetic interactions are intrinsically exchange-correlation effects, we will use a multireference configuration interaction method to compute them, namely, the selected active space plus single excitation (SAS+S) method [15].

*marie-bernadette.lepetit@neel.cnrs.fr

†andres.saul@cnrs.fr

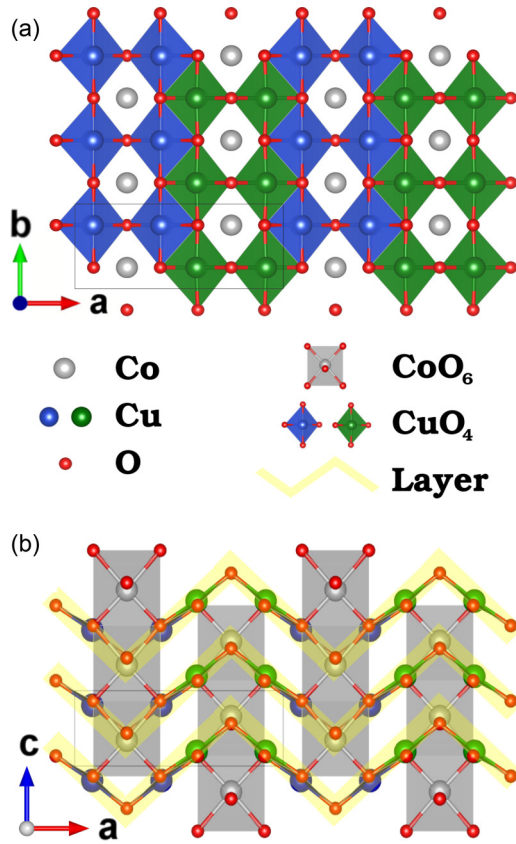


FIG. 1. Schematic of the crystal structure of CoCu_2O_3 . (a) along the \bar{c} and (b) \bar{b} axes. The Cu atoms form two-leg ladders along the \bar{b} direction, and there are two symmetry-related ladders along the \bar{a} direction. The Cu atoms were represented either in blue or in green to more easily visualize the two equivalent structural ladders. The Co atoms are in light gray and the O in red. Atomic structures were drawn with VESTA [14].

Indeed, this method ensures that the following effects are treated explicitly: (i) the correlation effect within the $3d$ magnetic orbitals, (ii) the ligand-to-metal charge transfers mediating the magnetic interactions, and (iii) the screening effects on all the previous configurations (as configuration-dependent hole-particle excitations and their coupling).

As such configuration interaction methods require the diagonalization of large matrices, they can only be used on formally finite-size systems. We, thus, designed for each magnetic integral, suitable fragments embedded in a set of renormalized charges [16] and total ions pseudopotentials (TIPS) [17] in order to reproduce the effects of the rest of the crystal on the quantum fragment. The TIPS reproduce the exclusion effects due to the electrons of the first layers surrounding the fragment, and the set of charges is chosen in order to reproduce the Madelung potential seen by the fragment with an error smaller than 0.1 meV. The quantum fragments were chosen in order to include the magnetic atoms associated with the desired interaction, their first coordination shell, and any additional bridging ligands.

The fragment orbitals were optimized within a complete active space self-consistent field [18] calculation on the $3d$ electrons of the magnetic atoms, using the MOLCAS

package [19]. We used a valence basis set of $3\zeta + P$ quality, associated with relativistic core pseudopotentials of the Stuttgart group [20]. The SAS+S calculations were then performed using the RELAXSE code [21]. The latter provides the fragment low-energy excitations from which the effective exchange integrals can be deduced.

The anisotropy calculations were performed using the same method on a single-ion embedded cluster for the spin-orbit-free description, and the RASSI/ANISO [22] modules of MOLCAS for the spin-orbit part. More details are available in the Supplemental Material [23].

The crystal structure used in all calculations is the room-temperature x ray given in Ref. [24].

B. Monte Carlo calculations

The MC simulations were performed on the model magnetic Hamiltonian derived from our *ab initio* effective exchange interactions and single-ion anisotropies. We computed both the order parameters and the magnetic transition temperatures. For this purpose we used the standard Metropolis algorithm [25] on a classical approximation of the spin Hamiltonian. The calculations were performed using supercells up to $10 \times 20 \times 20$ (24 000 magnetic atoms). The thermodynamical averages were performed with 4000 Monte Carlo steps per atom. More details are available in the Supplemental Material [23].

III. RESULTS OF THE *AB INITIO* CALCULATIONS

A. Magnetic integrals

The formal charge analysis of CoCu_2O_3 yields Cu^{2+} and Co^{2+} , corresponding, respectively, to $3d^9$ and $3d^7$ electronic configurations. The corresponding magnetic moments are $S_{\text{Cu}} = \frac{1}{2}$ and $S_{\text{Co}} = \frac{3}{2}$ because the Co ion is in a high-spin configuration (as expected for such ions and by continuity from the partially substituted compounds $\text{Mg}_{1-x}\text{Co}_x\text{Cu}_2\text{O}_3$ for $x = (0.05, 0.10, 0.15, 0.50)$ [26] and confirmed by our calculations).

The magnetic exchange interactions were obtained from the *ab initio* calculations by mapping the computed magnetic spectra onto the energy spectra of a Heisenberg Hamiltonian on the same fragments,

$$\hat{H} = - \sum_{\langle i,j \rangle} J_{ij} \hat{S}_i \cdot \hat{S}_j, \quad (1)$$

where \hat{S}_i and \hat{S}_j are the quantum spin operators associated with sites i and j , respectively. The J_{ij} are the effective exchange interactions, positive and negative values correspond, respectively, to ferromagnetic (FM) and antiferromagnetic (AFM) interactions.

In Fig. 1(b) one sees that the cobalt octahedra are located between two layers of copper ladders. However, magnetically they belong to only one of them. Indeed, the CuO_4 plaquettes define the orientation of the magnetic $d_{x^2-y^2}$ orbitals expected on the Cu^{2+} ions. Looking at Fig. 1 one can see that the CuO_4 plaquettes of only one of the layers point toward the Co^{2+} ion. As a result the Co^{2+} ions should be considered as belonging to the connecting layer of copper ladders [see Fig. 1(b)].

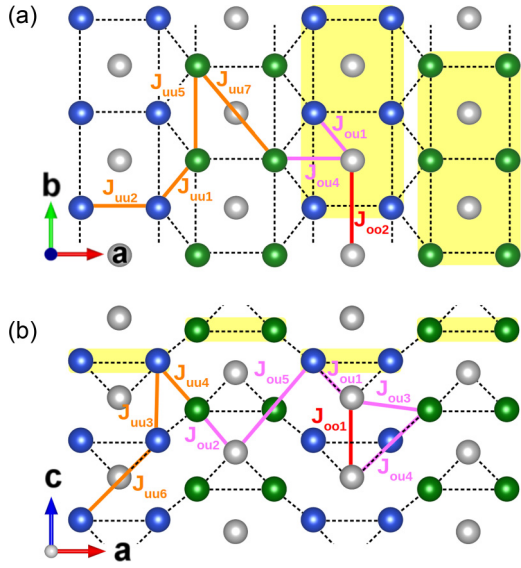


FIG. 2. Definition of magnetic interactions in CoCu_2O_3 , seen along the (a) \bar{c} and (b) \bar{b} directions. The Co atoms are in light gray, the Cu atoms are in blue and green, and the O atoms are masked. The Cu-Cu interactions are in orange, the Co-Cu interactions are in magenta, and the Co-Co interactions are in red. Dashed lines represent the puckered layers, and yellow boxes are a guide to identify structural ladders. Atomic structures were drawn with VESTA [14].

There are seven independent Cu-Cu interactions in CoCu_2O_3 , named, J_{uuX} (in orange in Fig. 2). Three of them are intraladder interactions: J_{uu2} is the ladder-rung interaction, J_{uu5} is the ladder-leg interaction, and J_{uu7} is the second-neighbor intraladder interaction. J_{uu1} is the in-plane interladder interaction. The last three are Cu-Cu interactions between the puckered planes, J_{uu3} , J_{uu4} , and J_{uu6} .

There are five Co-Cu interactions, named J_{ouX} , (in magenta in Fig. 2). The intralayer ones are J_{ou2} where the Co atom is between two rungs of a ladder and J_{ou4} where the Co atom interacts with the next-ladder nearest copper. The interlayer interactions are denoted J_{ou1} , J_{ou3} , and J_{ou5} [see Fig. 2(b)].

Finally, there are two Co-Co interactions (in red in Fig. 2), J_{oo1} along the \bar{c} axis and J_{oo2} along the \bar{b} axis.

The computed exchange interactions are presented in Table I. We can immediately see that the largest magnetic interaction is the AFM exchange along the ladders legs ($J_{uu5} = -123.43$ meV). When one looks at the ladder rungs (J_{uu2}), however, the interaction does correspond neither to the largest J nor to the largest contributions to the classical magnetic energy $-J\vec{S}_i \cdot \vec{S}_j$. Indeed, the next largest magnetic energy contribution is due to the Cu-Co AFM interactions (J_{ou4}); the interaction along the structural-ladder rungs being much smaller. The third energetic contribution comes from the Co-Co intralayer interactions, namely, J_{oo2} . As a result one should differentiate the magnetic ladders, based on J_{uu5} and J_{oo2} for the legs, J_{ou4} for the rungs from the structural ones. Indeed, these interactions draw a magnetic-interaction pattern of three-leg Cu-Co-Cu ladders (see Fig. 3), obtained by the exchange of the legs of neighboring structural ladders (yellow in Fig. 2). Finally, the next contribution to the magnetic

TABLE I. Effective exchange interactions (in meV) obtained from *ab initio* calculations, associated Heisenberg energy, and metal-metal distances (in angstroms). Negative values correspond to AFM interactions, and positive values correspond to FM ones.

| d (Å) | J_{ij} | $-J_{ij}\vec{S}_i \cdot \vec{S}_j$ | Nature | |
|--------------------|----------|------------------------------------|--------|-----------------------------------------|
| Cu-Cu intralayers | | | | |
| J_{uu5} | 3.980 | -123.43 | -30.86 | Leg structural ladders |
| J_{uu1} | 2.829 | 27.85 | 6.96 | Interstructural ladders |
| J_{uu2} | 3.118 | 9.75 | 2.44 | Rung structural ladders |
| J_{uu7} | 5.056 | 0.09 | 0.02 | Next-nearest-neighbor structural ladder |
| Cu-Cu interlayers | | | | |
| J_{uu3} | 3.198 | -0.42 | -0.10 | |
| J_{uu4} | 3.213 | -0.65 | -0.16 | |
| J_{uu6} | 4.466 | 1.94 | 0.49 | |
| Cu-Co interactions | | | | |
| J_{ou4} | 4.157 | -26.97 | -20.23 | Intralayer |
| J_{ou1} | 2.931 | 5.67 | 4.25 | Intralayer |
| J_{ou3} | 3.182 | 2.81 | 2.10 | Interlayer |
| J_{ou2} | 3.055 | 1.23 | 0.92 | Interlayer |
| J_{ou5} | 4.839 | 0.23 | 0.17 | Interlayer |
| Co-Co interactions | | | | |
| J_{oo2} | 3.980 | -4.22 | -9.50 | Leg type |
| J_{oo1} | 3.198 | -1.05 | -2.36 | Interlayer type |

energy comes from the FM Cu-Cu interladder (structural or magnetic) zigzag interactions (J_{uu1}).

Comparing CoCu_2O_3 to SrCu_2O_3 and to the other members of the family, they all have in common large AFM ladder leg interactions. The main differences are related to the ladder rungs and more specifically to the bending of the Cu-O-Cu angle in the structural-ladder rungs. Indeed, this angle is close to 180° in the SrCu_2O_3 and results in an AFM interaction of -150 meV [27] (of the same order of magnitude as the ladder leg one) responsible for the one-dimensional character of the compound, and the correspondence between the structural and magnetic two-leg ladders. On the contrary the CaCu_2O_3 system presents a large bending of the Cu-O-Cu

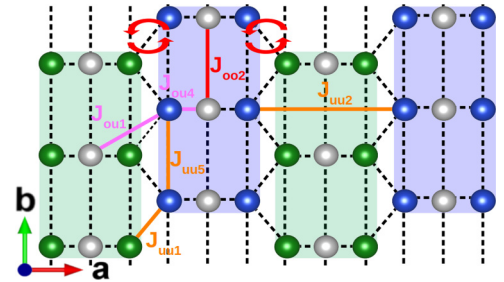


FIG. 3. Schematic of the magnetic interaction pattern in CoCu_2O_3 . This pattern is obtained from the structural pattern [Fig. 2(a)] by the exchange of the legs of neighboring ladders as pictured by the red arrows. The main interactions are added for easy comparison. The dashed black lines represent the magnetic pucker layers including the Co atoms, the dashed gray lines show the rungs of the structural ladders, and blue or green boxes show the magnetic ladders.

angle, namely, of 123° [28] in the structural-ladder rungs. It results in a strongly reduced magnetic interaction (nevertheless, still AFM (-11.5 meV) [27]) leading to a quasi-1D magnetic structure of coupled chains. In the present system the Cu-O-Cu angle is again reduced compared to the CaCu_2O_3 (105° [24]) and much closer to 90° , yielding an enhanced reduction of the AFM term, and resulting in a FM interaction of $J_{uu2} = 9.7$ meV. This result is in agreement with the ferromagnetic ordering, experimentally observed (along the rungs) by neutron diffraction on the MgCu_2O_3 compound [29] where the angle is also 105° [30].

To better understand the importance of the Cu-O-Cu angle bending, one should remember that the effective magnetic exchanges are the result of three terms [31]:

(1) a direct exchange term between the magnetic atoms (J_d), this term is always FM and depends exponentially on the metal-metal distance,

(2) a through-space (also named kinetic or Anderson's superexchange) superexchange term (J_{ss}), issued from electron transfers between the two magnetic atoms, this term is AFM and decreases exponentially with the metal-metal distance, it is, thus, very small in systems where the metal-metal bond is bridged by a ligand,

(3) Finally the through-bridge superexchange term (J_{sb}), issued from electron transfers between the bridging ligand and the magnetic atoms, this term is AFM and depends exponentially on the metal ligand distance and as the square of the cosine of the metal-ligand-metal angle (θ); it is the largest term in AFM bridged systems.

In a first approximation, the effective magnetic exchange can, thus, be assumed to be

$$J = \underbrace{J_d(d_{\text{Cu-Cu}})}_{\text{FM, scales as } e^{-ad}} + \underbrace{J_{sb}(R_{\text{Cu-O}}, \theta_{\text{Cu-O-Cu}})}_{\text{AFM, scales as } e^{-\beta R} \cos^2 \theta}. \quad (2)$$

The bending of the Cu-O-Cu angle, thus, increases the FM term J_d as it is associated with a reduction of the Cu-Cu distance. Simultaneously it strongly reduces the AFM through-bridge superexchange term when going from 180° where the latter is maximum to 90° where it cancels out. One, thus, sees that the Cu-O-Cu angle is a crucial parameter for the magnetic properties of the ACu_2O_3 family.

Let us now focus on the magnetic character of the A site in our compound. Structurally CoCu_2O_3 and MgCu_2O_3 are very similar. However, the magnetic character of the Co^{2+} ion transforms the coupled chain magnetic pattern found in the Mg compound into a coupled three-leg ladder system in CoCu_2O_3 (see Fig. 3). Let us remember that the second largest magnetic energy is brought by the copper cobalt J_{ou4} interaction and the next one by the Co-Co ladder legs (J_{oo2}).

Analyzing the interactions in the puckered layers a bit closer one sees that there are two frustrating magnetic interactions, namely, the J_{uu1} FM interactions between the ladders, and the FM J_{ou1} interactions between the Co atoms and the Cu atoms of the neighboring magnetic ladders (see Fig. 3). Both interactions bring frustration with the AFM interaction along the ladder legs.

Finally, the interactions between the magnetic puckered layers are conveyed by the FM J_{ou3} and AFM J_{oo1} . As can be

seen in Table I the remaining interactions can be considered negligible.

B. Anisotropy

As the Cu^{2+} ion is in a $S = 1/2$ quantum spin state, the anisotropy of the compound is due to the Co^{2+} ion. We, thus, computed the cobalt easy axes and zeroth-field splitting tensor on embedded CoO_6 fragments.

The zeroth-field splitting tensor is derived from the eigenstates and energies of the many-body *ab initio* electronic plus spin-orbit Hamiltonian on the CoO_6 embedded fragment, using the pseudospin method of Chiboratu and Ungur [22].

We found that in our system the main anisotropy axes are along the crystallographic directions, \vec{b} is the easy axis, and \vec{c} is the hard one. They are associated with a strong anisotropy. Indeed, the zeroth-field splitting tensor can be written as

$$\hat{H}_{\text{ZFS}} = \mathcal{D} \left[\left(\hat{S} \cdot \frac{\vec{b}}{b} \right)^2 - \frac{S(S+1)}{3} \right] + \mathcal{E} \left[\left(\hat{S} \cdot \frac{\vec{c}}{c} \right)^2 - \left(\hat{S} \cdot \frac{\vec{a}}{a} \right)^2 \right], \quad (3)$$

with $\mathcal{D} = -10.60$ and $\mathcal{E} = 2.10$ meV. These values are comparable to some of the strongest magnetic exchange interactions. As a consequence one can expect the anisotropy to play a major role in the magnetic ordering.

IV. MAGNETIC PROPERTIES

A. Magnetic order at $T = 0$ K

As previously seen, the three exchange interactions with the strongest energy contributions, namely, J_{uu5} , J_{ou4} , and J_{oo2} , form three-leg ladders along the \vec{b} direction that do not correspond to the structural ones (see Fig. 3). These three AFM interactions, (J_{uu5} , J_{ou4} , and J_{oo2}) do not bring any frustration resulting in antiferromagnetically ordered three-leg ladders. Moreover, the large anisotropy of the Co ions aligns the spins along the \vec{b} axis.

The next nonfrustrated contribution to the magnetic energy comes from the FM interaction J_{uu2} , which connects second-neighbor magnetic ladders, forming two independent magnetic puckered planes in the $(\vec{a}-\vec{b})$ directions. These two independent subsystems are pictured in blue and green in Fig. 3. One should note that the two subsystems are related by the 2_1^y or *i*-symmetry operations. The different planes are then connected by the AFM J_{oo1} and FM J_{ou3} interactions, leading to two magnetically independent 3D nonfrustrated subsystems. Both subsystems are associated with a $\vec{q} = (0, \frac{1}{2}, \frac{1}{2})$ propagation vector. The two subsystems are coupled by the remaining non-negligible exchange interactions (see Table I), namely, the FM J_{uu1} and J_{ou1} . These two interactions are frustrated and, thus, do not contribute to the magnetic energy in the proposed $T = 0$ magnetic order (see Fig. 4).

At this point the question is whether the above twofold degenerate magnetic ordering (pictured in Fig. 4) is the ground state. It is easy to show that these two magnetic orders

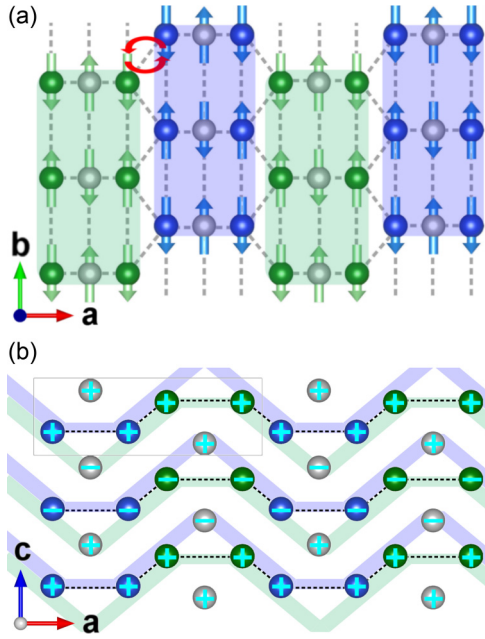


FIG. 4. Schematic of the magnetic structure of CoCu₂O₃. (a) Order on the puckered magnetic layers. (b) Order in the structural arrangement. The Co atoms are in light gray and the Cu in blue or green according to the magnetic subsystem they belong to. The latter are outlined by blue and green boxes. Atomic structures were drawn with VESTA [14].

correspond to minima of the classical magnetic energy: nil gradient and positive Hessian.

Let us note that both the CaCu₂O₃ [12] and the MgCu₂O₃ [29] compounds also exhibit degenerate ground states, however, with different subsystems and magnetic orders.

Doubly degenerate ground states are very rare in real compounds as any perturbation, coupling the two states, lifts the degeneracy. In CoCu₂O₃ such a coupling does not exist in the present crystallographic space group and unit cell. One can, however, see that to couple the two ground states and reduce the magnetic frustration, one should double the crystallographic cell along the \vec{b} direction. Indeed, such a symmetry reduction could allow lowering of the frustration brought by the inter-magnetic-ladder interactions J_{uu1} and J_{ou1} . Let us remember that spin-1/2 chains could exhibit spin-Peierls transitions and that the dominant magnetic interaction in CoCu₂O₃ is, by far, the AFM exchange along the Cu ladder leg. One can, thus, expect that such an effect is also at play in CoCu₂O₃ producing the dimerization that doubles the unit cell and lowers the energy.

Comparing the magnetic orders of CoCu₂O₃ with CaCu₂O₃ and MgCu₂O₃, one sees that in addition to different magnetic ladders as discussed in the previous section, these compounds also exhibit different propagation vectors. Indeed, CaCu₂O₃ is dominated by an incommensurate order $\vec{q} = (0.429, \frac{1}{2}, \frac{1}{2})$ [28] and MgCu₂O₃ by the commensurate $\vec{q} = (\frac{1}{2}, \frac{1}{2}, 0)$ [29] propagation vector. This is due to the non-magnetic character of the Ca and Mg ions that probably induce a weakly AFM interaction between the ladders, mediated by these closed-shell ions.

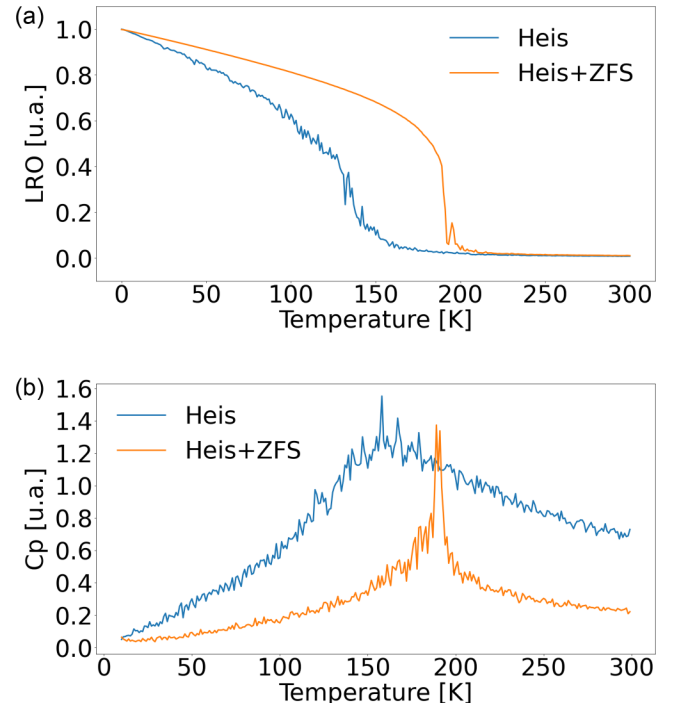


FIG. 5. Results of Monte Carlo simulations. (a) LRO and (b) specific heat versus temperature. The two curves represent our MC results with (orange) and without (blue) the Co²⁺ zeroth-field splitting contribution to the model Hamiltonian.

B. Magnetic properties at finite temperature

To study the thermodynamic properties at finite temperature, we performed classical MC simulations. We computed both the specific-heat C_p and the long-range-order parameter (LRO), characteristic of the $\vec{q} = (0, \frac{1}{2}, \frac{1}{2})$ magnetic order identified in the previous section. The calculation was performed using the Heisenberg Hamiltonian defined from the exchange interactions given in Table I, complemented with the zeroth-field splitting tensor of the Co ions as provided in Sec. III.

Figures 5(a) and 5(b) display, respectively, LRO and C_p as a function of temperature. When the Heisenberg and zeroth-field splitting terms are considered, one can see that both quantities (in orange in both panels) exhibit a clear transition at $T_N \simeq 190$ K confirming the magnetic order proposed in the previous section. The magnetic frustration brought by the inter-magnetic-ladder effective exchanges do not bring any noticeable canting of the spins in the MC results. All spins remain aligned along the \vec{b} direction. When decreasing the temperature we obtain a MC average energy of about -259.8 meV/cell, in good agreement with the theoretical ground-state classical magnetic energy,

$$\begin{aligned}
 E_{\text{cell}} = & (2J_{oo2} + 2J_{oo1}) S_{\text{Co}}^2 + 2\mathcal{D} \left[S_{\text{Co}}^2 - \frac{S_{\text{Co}}(S_{\text{Co}} + 1)}{3} \right] \\
 & + (4J_{ou4} - 4J_{ou3} + 4J_{ou5}) S_{\text{Cu}} S_{\text{Co}} \\
 & + (4J_{uu5} - 2J_{uu2} + 4J_{uu6} + 4J_{uu3} + 4J_{uu7}) S_{\text{Cu}}^2 \\
 = & -260.2 \text{ meV/cell.} \tag{4}
 \end{aligned}$$

As suggested in the previous section the frustrating interactions J_{uu1} , J_{ou1} , (as well as J_{ou2} and J_{uu4}) do not contribute to the energy. The very small interactions, neglected in our previous analysis, namely, J_{uu6} , J_{ou5} and J_{uu7} , have positive contributions to energy, i.e., these interactions are frustrated, but their effect is negligible.

Let us note that, despite the quantum character of the spin-1/2 Cu ions, the obtained transition temperature is close enough to the $T_N = 215$ K value observed in magnetic susceptibility and specific-heat measurements [13]. In fact, the Co anisotropy plays a major role, its inclusion in the model Hamiltonian breaks the rotational symmetry, transforming CoCu_2O_3 in an Ising-like magnetic system. Indeed, in MC simulations where only the exchange interactions are taken into account (see the blue curves in Fig. 5), long-range magnetic order is obtained by the 3D character of the Heisenberg Hamiltonian provided by the interplane interactions J_{uu3} , J_{ou3} , and J_{ou1} . As the leading interactions of the system are quasi-2D, the symmetry breaking of the rotational invariant Hamiltonian is numerically more difficult to achieve, and the transition appears less clear in Fig. 5 but definitively takes place at lower temperature ($T_N \approx 150$ K). Nevertheless, the magnetic order remains identical, apart from the general spin orientation.

V. CONCLUSION

In this paper we theoretically determined the magnetic order and transition temperature of the CoCu_2O_3 ladder compound. We first computed the effective magnetic interactions and anisotropy parameters using an *ab initio* multireference configuration interactions method (SAS + S [15,21]). With these parameters, we constructed a model Hamiltonian that has been used to determine the magnetic order at $T = 0$ K and at finite temperature.

Compared to other members of the ACu_2O_3 family the CoCu_2O_3 compound is characterized by puckered layers with a large folding angle, and by a supplementary magnetic ion (Co^{2+}). These two aspects have strong consequences on the magnetic properties of the system. Indeed, our results allow us to predict that the magnetic ladders strongly differ from those of the other members of the family. First, not only they

are not identical to the structural ladders, but they exhibit three and not two legs. Second, these magnetic ladders are strongly connected, both in the layers and between the layers, resulting in a twofold degenerated ground state. Finally, there is the strong Co^{2+} easy axis along the \vec{b} direction that not only reduces the otherwise infinite degeneracy to a twofold one, but also explains the strong increase (compared to the other members of the family) of the temperature at which the long-range magnetic order sets in. It would be nice if our predicted magnetic order could be experimentally verified, for instance, by neutrons diffraction.

We would like to conclude on the magnetic frustration responsible for the degenerated ground state. This degeneracy is due to the existence of two 3D subsystems only coupled by frustrated interactions. One, thus, expects that a structural distortion should occur to lower this frustration and couple the two subsystems. Our analysis yields that the expected distortion should be a doubling of the unit cell along the \vec{b} direction. Indeed, not only such a symmetry breaking would lower the magnetic frustration, but it would also allow the Cu chains (ladder legs) to display a spin-Peierls transition as expected in spin-1/2 chains. Such a transition is reasonably expected at, or close to, the magnetic ordering temperature, however, no structural transition has been seen in x-ray diffraction in the 115–300 K range as stated in Ref. [13]. One should, however, remember that the energy associated with the magnetic frustration (issued from J_{uu1} and J_{ou1}) is small compared to the other energy scales in the system. As a result the atomic displacements associated with the symmetry breaking can be expected to remain weak, and, thus, difficult to see with diffraction techniques (as was learned over the past years by the study of multiferroic systems). Most probably only lattice dynamic studies will be able to clarify this point.

ACKNOWLEDGMENTS

We acknowledge financial support from the ANR HTH-PCM. This work was performed using computer resources obtained from GENCI-IDRIS and CRIANN under Projects No. 91842 and No. 2007013.

-
- [1] J. G. Bednorz and K. A. Müller, *Z. Phys. B: Condens. Matter* **64**, 189 (1986).
 - [2] Z. Hiroi, M. Azuma, M. Takano, and Y. Bando, *J. Solid State Chem.* **95**, 230 (1991).
 - [3] M. Azuma, Z. Hiroi, M. Takano, K. Ishida, and Y. Kitaoka, *Phys. Rev. Lett.* **73**, 3463 (1994).
 - [4] E. Dagotto and T. M. Rice, *Science* **271**, 618 (1996).
 - [5] A. W. Sandvik, E. Dagotto, and D. J. Scalapino, *Phys. Rev. B* **53**, R2934 (1996).
 - [6] M. Azuma, H. Yoshida, T. Saito, T. Yamada, and M. Takano, *J. Am. Chem. Soc.* **126**, 8244 (2004).
 - [7] K. Sparta, A. Löffert, C. Gross, W. Abmus, and G. Roth, *Z. Krist.* **221**, 782 (2006).
 - [8] R. Achleitner, H. G. Evertz, M. Imada, R. Gamillscheg, and P. Mohn, *Phys. Rev. B* **88**, 214422 (2013).
 - [9] J.-H. Hu and H. L. Johnston, *J. Am. Chem. Soc.* **75**, 2471 (1953).
 - [10] J. B. Forsyth, P. J. Brown, and B. M. Wanklyn, *J. Phys. C* **21**, 2917 (1988).
 - [11] T. Zeiske, H. Graf, H. Dachs, and K. Clausen, *Solid State Commun.* **71**, 501 (1989).
 - [12] M. Wolf, K.-H. Müller, D. Eckert, S.-L. Drechsler, H. Rosner, C. Sekar, and G. Krabbes, *J. Magn. Magn. Mater.* **290-291**, 314 (2005).
 - [13] C. Sekar, S. Paulraj, G. Krabbes, M. Kanagaraj, S. Arumugam, and R. S. Kumar, *J. Magn. Magn. Mater.* **323**, 3033 (2011).
 - [14] K. Momma and F. Izumi, *J. Appl. Cryst.* **44**, 1272 (2011).
 - [15] A. Gellé, J. Varignon, and M.-B. Lepetit, *Europhys. Lett.* **88**, 37003 (2009).

- [16] A. Gellé and M.-B. Lepetit, *J. Chem. Phys.* **128**, 244716 (2008).
- [17] N. W. Winter, R. M. Pitzer, and D. K. Temple, *J. Chem. Phys.* **86**, 3549 (1987).
- [18] B. O. Roos, P. R. Taylor, and P. E. Sigbahn, *Chem. Phys.* **48**, 157 (1980).
- [19] F. Aquilante, J. Autschbach, R. K. Carlson, L. F. Chibotaru, M. G. Delcey, L. De Vico, I. Fdez. Galván, N. Ferré, L. M. Frutos, L. Gagliardi, M. Garavelli, A. Giussani, C. E. Hoyer, G. Li Manni, H. Lischka, D. Ma, P. A. Malmqvist, T. Müller, A. Nenov, M. Olivucci, T. B. Pedersen, D. Peng, F. Plasser, B. Pritchard, M. Reiher, I. Rivalta, I. Schapiro, J. Segarra-Martí, M. Stenrup, D. G. Truhlar, L. Ungur, A. Valentini, S. Vancoillie, V. Veryazov, V. P. Vysotskiy, O. Weingart, F. Zapata, and R. Lindh, *J. Comput. Chem.* **37**, 506 (2016).
- [20] M. Dolg, U. Wedig, H. Stoll, and H. Preuss, *J. Chem. Phys.* **86**, 866 (1987).
- [21] E. Rebolini and M.-B. Lepetit, *J. Chem. Phys.* **154**, 164116 (2021).
- [22] L. F. Chibotaru and L. Ungur, *J. Chem. Phys.* **137**, 064112 (2012).
- [23] See Supplemental Material at <http://link.aps.org/supplemental/10.1103/PhysRevB.106.224402> for a detailed description of the calculations workflow and details.
- [24] H. Müller-Buschbaum and A. Tomaszewska, *Z. Kristallogr.* **196**, 121 (1991).
- [25] N. Metropolis, A. W. Rosenbluth, M. N. Rosenbluth, A. H. Teller, and E. Teller, *J. Chem. Phys.* **21**, 1087 (1953).
- [26] Q. Zhou, H. Suzuki, and T. Yamadaya, *J. Low Temp. Phys.* **115**, 229 (1999).
- [27] E. Bordas, C. d. Graaf, R. Caballol, and C. J. Calzado, *Theor. Chem. Acc.* **116**, 535 (2006).
- [28] V. Kiryukhin, Y. J. Kim, K. J. Thomas, F. C. Chou, R. W. Erwin, Q. Huang, M. A. Kastner, and R. J. Birgeneau, *Phys. Rev. B* **63**, 144418 (2001).
- [29] M. Winkelmann, H. A. Graf, and N. H. Andersen, *Phys. Rev. B* **49**, 310 (1994).
- [30] H. Drenkhahn and H. Müller-Buschbaum, *Z. Anorg. Allg. Chem.* **418**, 116 (1975).
- [31] M.-B. Lepetit, in *Recent Research Developments in Quantum Chemistry*, 3 (Transword Research Network, Trivandrum, India, 2002), p. 143.